# KINEMATICS OPTIMIZATION FOR A FLAPPING-WING MICRO AIR VEHICLE

**Thomas Rakotomamonjy** * **Thierry Le Moing** *
**Mustapha Ouladsine** **

* *Office National d'Études et de Recherches Aérospatiales (ONERA), Base aérienne 701, 13661 Salon de Provence, France*
** *Laboratoire des Sciences de l'Information et des Systèmes (LSIS), Domaine Universitaire de Saint-Jérôme, 13397 Marseille, France*

Abstract: A flight-dynamics oriented simulation model of a flapping-wing Micro Air Vehicle (MAV) has been developed. This concept is based on flapping flight performed in nature by insects or hummingbirds. An optimization of the flapping kinematics of the wing has been led, in order to maximize the mean lift and thus the payload. A neural network has been designed to reproduce the function shape of the wings movements, and the weights have been optimized using a genetic algorithm. Results show a lift gain from 30 to 40%, and corroborate also some mechanisms shown up through experiments. 

Keywords: aerospace engineering, simulation, optimization, neural networks, genetic algorithms

## 1. INTRODUCTION

The Micro Air Vehicles (MAVs) represent nowadays a large field of investigation, due to their interests in both civil and military domains : such small and autonomous devices could be used for inspecting high monuments, monitoring risks of forest fires, or more generally for interventions in narrow and hazardous environments, where it would be dangerous to send a human agent. Concerning the military domain, MAVs prove their interest in being able to be both fully autonomous and carriable by a single infantryman, with foreseen applications such as rescuing or reconnaissance (*"behind the hill"*). From now on, the studied concepts were mainly based on fixed or rotary wings (helicopter-type). The proposed model features flapping wings, which reproduces the flight of insects or hummingbirds. The advantages are on one hand a greater manœvrability, particularly at low speeds or even for hovering, allowing indoor missions, and on the other hand a more discrete acoustical spectrum (in comparison with rotary wings), which one is no longer centered around one single frequency - the rotation frequency - but more spread. The work presented here are led in parallel with the *Projet de Recherches Fédérateur* (federative research project, hereafter PRF) REMANTA, conducted at the ONERA (Descatoire *et al.*, 2003), and which aims to enlarge the scientific or technical knowledges and methods in the field of flapping wings MAVs.

First, a review of the available works concerning the theory of natural flapping flight and its applications to artificial aerial devices has been done, in a bibliographic study. It has allowed us to draw out two possible configurations for this kind of flight : bird-like flight, in which the wings flap at low/medium frequency within a near ver-

tical plane, and insect-like flight, where the wings flap at a higher frequency within a horizontal or slightly inclined plane, generating lift in both strokes directions (back and forth). This last kind of flapping flight is also typical of hummingbird, who is the only bird able to perform mastered hovering flight.

Many authors have worked by now on understanding the animal flight, particularly during the last century. The main encountered obstacle was the inability of the classical aerodynamic mechanisms known by then to explain the insect flight : applicating classical theorems for a pair of insect wings gave indeed a too weak lift to sustain the flying animal (hence the famous paradox *bumblebees can't fly*). Weis-Fogh was one of the first to propose unstationnary aerodynamic mechanisms from experiments, which would explain where came the missing lift from (Weis-Fogh, 1972; Weis-Fogh, 1973). Let us also mention the many works of Ellington on aerodynamics of hovering flight (Ellington, 1984) and of Norberg, who proposed a model inspired by the Rankine-Froude momentum theory to calculate the lift of a hovering bat (Norberg, 1993).

The last progress made in understanding aerodynamics of insect flight came from Dickinson, who simulated the flow around a fly wing *Drosophila melanogaster* (Dickinson *et al.*, 1999) using a scaled wing model flapping in mineral oil, in order to keep the low Reynolds ($Re$) number (a few hundreds) characteristic of this type of flight. Three specific aerodynamic effects have been shown up as the cause of a lift gain at low $Re$ : the circulation generated by the rotation of the wing at the end of a stroke, the delayed stall due to the instationnarity of the movement, and finally the wake capture, as the wing re-enters the flow it has previously disturbed.

## 2. PRESENTATION OF THE SIMULATION MODEL

### *2.1 Description*

This model was initially written by T. Le Moing (ONERA) in C++ object language. It computes at each time step the values of the internal variables such as velocities, forces and momentums as a function of the controllable inputs. There are three independent inputs for each wing, corresponding to the three possible rotations of the wing with respect to the body : $\xi$ is the angle of the stroke plane ($\xi = 0$ when the wing flaps vertically and $\xi = \pi/2$ when it flaps horizontally), $\lambda$ is the angle locating the wing within the stroke plane and $\nu$ is the angle of rotation of the wing around its longitudinal axis (see fig. 1).

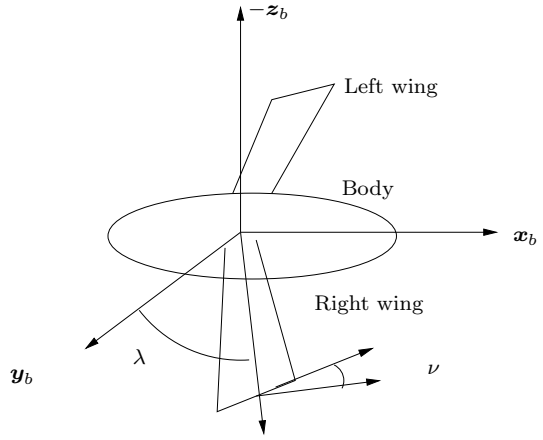


Fig. 1. Definition of the position angles (here $\xi = \pi/2$)

A local type approach has been chosen for this model, dividing the wing in slices according to 2-D approach. The wing kinematics and the global motion of the MAV allow to compute the local aerodynamic velocities for each wing element. This defines a local aerodynamic frame, and thus a corresponding aerodynamic incidence. The elemental forces are then calculated, according to the analytical models adopted to represent the different components of the aerodynamic force (Walker, 2002; Fung, 1993; Dickinson *et al.*, 1999), and those efforts are summed along the wing, giving a global force and momentum applied to the mass center of the MAV.

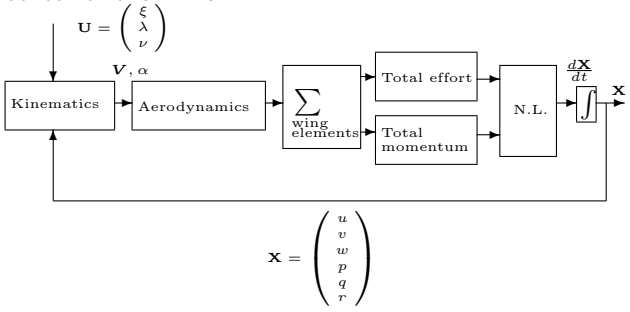


Fig. 2. Structure of the simulation model

Although such a local bidimensional approach does not take account for the transversal components of the flow, it has been stated that it was sufficient enough to reproduce the commonly observed phenomena for this case of flight, and furthermore that flight dynamics-oriented problems, such as simulation and control, could be more easily treated than with the CFD-based methods (Sane and Dickinson, 2002). At last, the total dynamic components (effort and momentum) are integrated within an inertial frame to give - according to Newton's first law (NL) - the state vector $\mathbf{X}$, whose components define the kinematic of the MAV : three translational velocities $u$, $v$, $w$ along each axis of the earth-bound inertial frame and three rotational velocities $p$, $q$, $r$ (respectively roll, pitch and yaw).

$$\mathbf{X} = {}^t(u\ v\ w\ p\ q\ r) \quad (1)$$

An overview of the structure of this model is given on fig. 2.

### *2.2 Validation*

Different validation steps have classically been led, in order to prove the pertinence of the complete simulation model (Rakotomamonjy *et al.*, 2004). In particular, some comparisons have been made between this model and previous results given by measurements on experimental devices. As an example, one main result obtained by Dickinson (Dickinson *et al.*, 1999) is the influence of the timing rotation with respect to the flapping of the wing : it has been shown that if the rotation of the wing begins slightly before the end of the stroke, some extra lift is generated, which is clearly visible as a peak on the vertical force records. On the contrary, if this rotation occurs after the beginning of the reverse stroke, it induces a loss of lift. Fig. 3 shows the same type of experiment done using our complete simulation model. The inputs $\lambda$ (wing flapping angle) and $\nu$ (wing rotation angle) are respectively modelled with a triangular-shaped signal (which corresponds to a constant angular velocity during each stroke), and a square-shaped signal, to ensure a constant incidence for a stroke. The aforementioned functions are equal to

$$\Delta_s(t) = \tanh[k_r \cos(\omega t + \phi)]$$

for $\nu$ ($k_r$ being a parameter influencing the slope of the front and back edges of the signal) and

$$\Delta_t(t) = \int \Delta_c(t)dt$$

for $\lambda$. The chosen configuration is based on the specifications of a fictitious MAV, inspired by the statistics of animal flight : a total wingspan of $2b = 15$ cm, a mass of $m = 30$ g and a flapping frequency of $f = 40$ Hz. Each wing is composed of $n = 10$ elements.

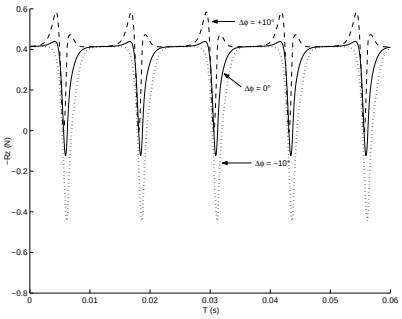


Fig. 3. Effect on the timing of wing rotation on total lift

Fig. 3 shows clearly that the results are close to those obtained experimentally : a phase advance and a phase delay of $\nu$ with respect to $\lambda$ cause respectively a gain and a loss of lift in comparison to the nominal settings (sign $-$ in front of $R_z$ is due to the downwards orientation of the vertical axis $\mathbf{z_n}$, as it is done conventionally in flight mechanics). This suggests the future usefulness of a differential control of the phase of the rotation of each wing, which would generate a different lift between the wings and thus a roll momentum, a strategy that some authors think already used by real insects to quickly change direction (Taylor, 2001).

## 3. OPTIMIZATION

After the model has been validated with arbitrary wing movements, an optimization of those kinematics has been undertaken. The chosen criterion in this study is the mean lift in hovering flight, since it is directly related to the maximum weight of the MAV and thus to the admissible payload (which includes for a MAV sensors, batteries but also actuators and navigation systems). Let $J$ be this criterion : $J = -\bar{R}_z$ (again, the minus sign corresponds to the downwards orientation of $\mathbf{z_n}$, according to flight mechanics conventions. Due to the periodical nature of the wings movements, the problem has been reduced over one flapping period (including down- and upstroke). The problem is then to find the kinematics $\lambda(t)$ or $\nu(t)$ which minimize $J$ over a period.

### *3.1 Input modelling*

The complexity of the model, mainly due to its nonlinear components, makes it very hard to reach an optimal flapping function expressed under an analytical form, as the solution of a functional equation. That is why this potential solution has been modelled under a parametric form, thus transforming a continuous-time optimal control problem into a non-linear programming problem. The question is now not to restrain too much the space of solutions, by imposing a certain form to the desired function (triangular, square...). The candidates functions were consequently modelled using neural networks, with the idea that a complex enough network could reproduce a large class of admissible functions. The *Neural Network* MATLAB®toolbox was used to represent, initialize and learn the network.

The first step is to choose an adapted network structure. The more complex the network is, the more various signals it can represent, but the optimization will in this case be less efficient, because of the high number of parameters involved : the compromise is to find the minimal network representing as many function shapes as possible suiting the specifications. Observations of natural

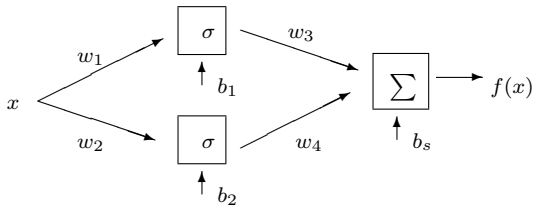


Fig. 4. Structure of the chosen network

insect wing kinematics have shown that the geometrical incidence remains nearly constant during a stroke, before the wing revolves and begins the next stroke. As a consequence, a square-shaped function was used as a basis for the rotation angle $\nu(t)$. But we have to consider also more classical functions, such as trigonometric ones for example : the chosen network must then be able to reproduce square $\nu_s = \tanh(k_r \cos \omega t)$ as well as cosine $\nu_c = \cos \omega t$ functions. After a few searches, we found that the minimal network reproducing both kind of signals features 2 layers, with 2 neurons on the hidden layer (input layer) and 1 neuron on the output layer. This network is shown on fig. 4. The neurons on the hidden layer have a sigmoid transfer function $\sigma(u) = \frac{1}{1+e^{-u}}$, and the output one a linear transfer (and acts just as a summing element). The weights $\{w_i\}_{i=1\ldots4}$ on each connection plus the biases give a total of $4 + 3 = 7$ parameters to be optimized.

The learning uses the retropropagation method, available in the above-mentioned toolbox. The results of learning of $\nu_s$ and $\nu_c$ during one period (given the periodic nature of the model inputs) are shown on fig. 5.

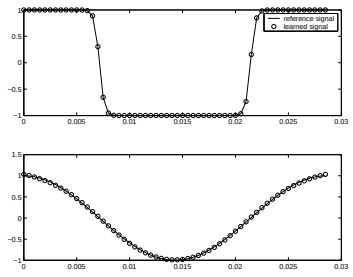


Fig. 5. Learning of $\nu_s$ and $\nu_c$

The chosen network appears able to reproduce those function shapes, as well as some others, which were not represented here, such as trapeze-shaped functions, where the junction between the constant floors are made using sine or polynomial arcs. The same operation is performed to model the flapping angle $\lambda(t)$ : this time, a total of 4 neurons on the hidden layer was necessary to reproduce the largest class of shapes.

### *3.2 Optimization algorithm*

Let $n$ be the number of neurons on the hidden layer of the network. $\{w_i\}_{i=1\ldots n}$ are the input weights, $\{w_i\}_{i=n\ldots2n}$ the output weights, $\{b_i\}_{i=1\ldots n}$ the neuron biases and $b_s$ the output bias. Let also $\mathbf{\Theta} = (\{w_i\}_{i=1\ldots2n}, \{b_i\}_{i=1\ldots n}, b_s)$ be the parameters array subject to optimization, $\hat{\mathbf{\Theta}}$ the optimum value, and $f_{\mathbf{\Theta}}(t)$ the corresponding function, which can be directly expressed :

$$f_{\mathbf{\Theta}}(t) = \sum_{i=1}^{n} \frac{w_{i+n}}{1 + e^{-(w_i t + b_i)}} + b_s \qquad (2)$$

At first standard optimization algorithms (Newton and Sequential Quadratic Programming methods) have been used to find $\hat{\mathbf{\Theta}}$. But the results were very dependant upon the initialization point $\mathbf{\Theta}_0$, and although the algorithm converged properly, the optimal array $\hat{\mathbf{\Theta}}$ and thus the corresponding kinematics and mean lift were different for many different values of $\mathbf{\Theta}_0$. This observation was confirmed by studying the sensitivity of the lift $-\bar{R}_z$ with respect to the different components of $\mathbf{\Theta}$. Figures 6 and 7 show the values of $-\bar{R}_z$ as a function of $(w_3; w_4)$ and $(b_1; b_2)$ respectively. The undulating shape of the surfaces and the many peaks correspond to local optima, in which a classical optimization algorithm can easily be trapped. That is why a genetic algorithm (GA) was used to try to override those local optima. The principle of this type of algorithm (Ouladsine *et al.*, 1995) is to generate a population of individuals, each one corresponding to a value of $\mathbf{\Theta}$. The population is then mixed, each individual having the ability to recombine his genes (the components of $\mathbf{\Theta}$) with a randomly selected other individual to try to find a better candidate to improve $J$.

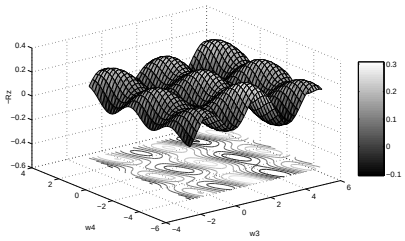


Fig. 6. Projection of $-\bar{R}_z$ within $(w_3; w_4)$ plane

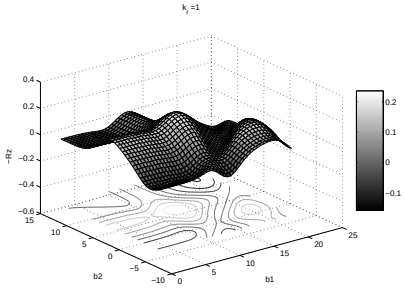


Fig. 7. Projection of $-\bar{R}_z$ within $(b_1; b_2)$ plane

Since this algorithm does not take any explicit constraint into account, one has to find the way

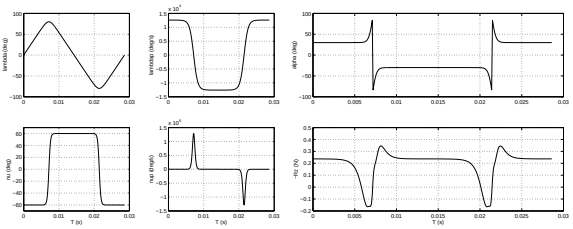

(a) Inputs $\lambda, \nu$ (b) Outputs $\alpha, -R_z$

Fig. 8. Reference inputs $\lambda_r$ et $\nu_r$

to express the necessity for the optimal solution to be periodic, *i.e.* $f_{\hat{\mathbf{\Theta}}}(0) = f_{\hat{\mathbf{\Theta}}}(T)$. This condition is then equivalent to (eq. 2) :

$$\sum_{i=1}^{n} \frac{w_{i+n}}{1+e^{-(w_i T+b_i)}} - \sum_{i=1}^{n} \frac{w_{i+n}}{1+e^{-b_i}} = 0 \qquad (3)$$

and it is now possible to express one chosen parameter as a combination of the other ones, for instance the last output weight $w_{2n}$ :

$$w_{2n} = -\frac{\sum_{i=1}^{n-1} w_{i+n} \left( \frac{1}{1+e^{-(w_i T+b_i)}} - \frac{1}{1+e^{-b_i}} \right)}{\left( \frac{1}{1+e^{-(w_n T+b_n)}} - \frac{1}{1+e^{-b_n}} \right)} \qquad (4)$$

thus reducing the dimension of the parameter space. Others methods of global optimization based on heuristical algorithms have also been tested, such as random adaptive search and simulated annealing, but we will focus here on the results given by the GA.

## 4. RESULTS

A reference case was defined using standard functions for the flapping angle $\lambda_r(t)$ and the rotation angle $\nu_r(t)$, defined respectively as :

$$\nu_r(t) = \tanh\left(10\cos\frac{2\pi t}{35}\right) \qquad (5)$$

$$\lambda_r(t) = \int_0^t \tanh\left(4\cos\frac{2\pi u}{35}\right) du \qquad (6)$$

Those functions and their respective time derivatives are represented on fig. 8(a), and the corresponding local aerodynamic incidence $\alpha$ and lift $-R_z$ on fig. 8(b). Those functions were arbitrarily chosen after studying the kinematics of many flying animals in nature. The corresponding mean lift over a period is $|\bar{R}_z|_r = 0.1994$ N, and the stroke plane is horizontal ($\xi = \pi/2$, see fig. 1).

First the rotation angle $\nu(t)$ was optimized, $\lambda$ being equal to $\lambda_r$. The result is shown on fig. 9. The mean lift is $|\bar{R}_z| = 0.2649$ N, which represents a gain of about 33% in comparison with the reference case. The optimal function shape is close to the standard one, but it is very interesting to notice how these results fit with previously observed behaviours : the optimal function shows a phase

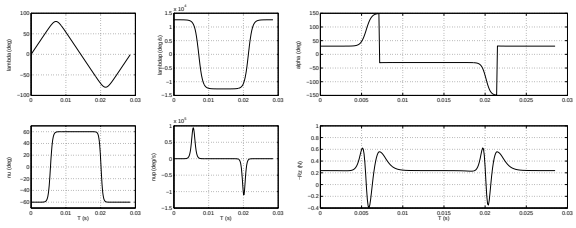

(a) Inputs $\lambda, \nu$ (b) Outputs $\alpha, -R_z$

Fig. 9. Optimization of $\nu$

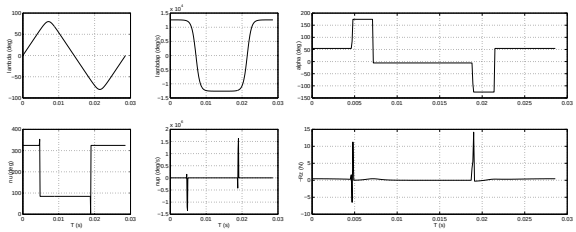

(a) Inputs $\lambda, \nu$ (b) Outputs $\alpha, -R_z$

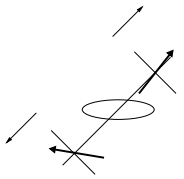

(c) Wing chord motion (arrow=leading edge)

Fig. 10. Optimization of $\nu$, $\xi = 45^\circ$

lead ($+18.44^\circ$) with respect to the reference one, which was not dephased. This corroborates the fact that an advanced rotation can bring an extra lift, in opposition with symmetrical kinematics, as observed with experimental devices such as *Robofly* (Dickinson *et al.*, 1999). Another significative point is that this phase lead did not appear explicitly within the model of the function : the weights of the neural network are indeed not directly interpretable in terms of physical components of the output function such as amplitude or phase.

The same method was applied for an inclined stroke plane : $\xi = 45^\circ$. This configuration is also frequent among the natural flyers, in particular for the *Odonates* (Wakeling and Ellington, 1997). The results are shown on fig. 10. This time, the rotation angle is dissymmetrical ($\nu_{\max} \neq -\nu_{\min}$), a feature also present in nature when the stroke plane is inclined. But this optimal shape features a great rotation amplitude of the wing (it performs 3/4 of a complete rotation around its axis, see fig. 10(c)) that is not found in animal flight, because of some inherent articular limitations.

The genetic algorithm did not give acceptable results for the optimization of $\lambda$ using the standard criterion : the optimal function presented

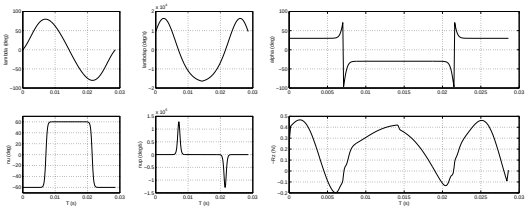

(a) Inputs $\lambda, \nu$ (b) Outputs $\alpha, -R_z$

Fig. 11. Optimization of $\lambda$ while limiting $\dot{\lambda}_{\max}$

very sharp variations and, besides the fact that the corresponding flapping speed $\dot{\lambda}$ would have been unreachable by any physical actuator, the inner nonlinearities of the model generated too many singular points during the simulation. The criterion was then modified to explicitly limit the peaks of $\dot{\lambda}$, by addition of a penalty term :

$$\tilde{J} = \alpha J + e^{\beta|\dot{\lambda}|_{\max}} \tag{7}$$

where $\alpha$ and $\beta$ are weighting coefficients. Fig. 11 shows the result obtained for $\alpha = 1$ and $\beta = 0.1$. This time the optimal function shape is much smoother, and close to a sinusoid. The lift gain is quite important : $|\bar{R}_z| = 0.2794$ N, or $+40\%$, which suggests that this function shape might be preferred over the triangular reference one $\lambda_r$ in further simulations. This type of kinematics would also be more convenient to implement on a real MAV, by using for example a steady oscillating resonant structure to drive the flapping.

## 5. CONCLUSION AND PERSPECTIVES

A simulation model has been previously developed for a flapping wing Micro Air Vehicle, which includes the specific aerodynamic effects for low-Reynolds flapping flight. The wing kinematics, defined as the inputs of the model, have been modelled using neural networks designed to reproduce the widest class of suitable function shapes. The flapping angle $\lambda(t)$ and the rotation angle $\nu(t)$ have been modelled with two single hidden layer network, having respectively 2 and 4 neurons on that layer. Then a genetic algorithm has been used to find the optimal kinematics so as to maximize the mean lift and thus the available payload, without being trapped in the many local optima. The result shows close similarities to previously obtained experimental results, in particular the fact that a lead advance of $\nu$ (rotation) with respect to $\lambda$ (flapping) brings an extra lift. The mean lift was improved by 30 to 40% in comparison with a reference case. Since this model can simulate the 6-degrees of freedom motion of the MAV, a similar procedure could be used for longitudinal flight (e.g. to maximize the forward speed). Those results are a useful help to design a flapping wing MAV, the next step being the development of suitable nonlinear control methods with this model.

## REFERENCES


Descatoire, F., Th. Le Moing, F. Bruyant and A. Morlière (2003). PRF REMANTA : Analyse de concepts de microdrones à ailes vibrantes. Rapport technique 7/06779. ONERA / DPRS - Ressources générales.

Dickinson, M.H., F.-O. Lehmann and S.P. Sane (1999). Wing rotation and the aerodynamic basis of insect flight. *Science* **284**, 1954–1960.

Ellington, C.P. (1984). The aerodynamics of hovering insect flight. *Philosophical transactions of the Royal Society of London. Biological sciences* **305**(1122), 1–181.

Fung, Y.C. (1993). *An introduction to the theory of aeroelasticity*. Dover Publications. New York.

Norberg, U.M. (1993). The cost of hovering and forward flight in a nectar feeding bat, *glossophaga soricina*, estimated from aerodynamic theory. *Journal of Experimental Biology* **182**, 207–227.

Ouladsine, M., F. Bicking and G. Bloch (1995). Identification of constrained dynamic-systems by genetic type algorithm. In: *Proceedings of the Artificial Intelligence in Real Time Control*. Bled.

Rakotomamonjy, T., T. Le Moing and M. Ouladsine (2004). Simulation model of a flapping-wing micro air vehicle. In: *First European Micro Air Vehicle Conference and Flight Competition (EMAV)*. Braunschweig.

Sane, S.P. and M.H. Dickinson (2002). The aerodynamic effects of wing rotation and a revised quasi-steady model of flapping flight. *Journal of Experimental Biology* **205**, 1087–1096.

Taylor, G.K. (2001). Mechanics and aerodynamics of insect flight control. *Biological Reviews of the Cambridge Philosophical Society* **76**(4), 449–471.

Wakeling, J.M. and C.P. Ellington (1997). Dragonfly flight. ii. velocities, accelerations and kinematics of flapping flight. *Journal of Experimental Biology* **200**, 557–582.

Walker, J.A. (2002). Rotational lift : something different or more of the same ?. *Journal of Experimental Biology* **205**, 3783–3792.

Weis-Fogh, T. (1972). Energetics of hovering flight in hummingbirds and in drosophila. *Journal of Experimental Biology* **56**, 79–104.

Weis-Fogh, T. (1973). Quick estimates of flight fitness in hovering animals, including novel mechanisms for lift production. *Journal of Experimental Biology* **59**, 169–230.

Żbikowski, R. (2002). On aerodynamic modelling of an insect-like flapping wing in hover for micro air vehicles. *Philosophical Transactions of the Royal Society of London. Mathematical, Physical and Engineering Sciences* **360**, 273–290.